JOURNAL OF AIRCRAFT
Vol. 32, No. 1, January–February 1995

Dynamic Investigation of the Angular Motion of a Rotating Body-Parachute System

D. Levin* and Z. Shpund†
Technion—Israel Institute of Technology, Haifa 32000, Israel

The modern design of parachute-payload systems that undergo specific trajectories has to cope with dynamic behavior characteristics, which were of secondary importance in the past. Static and dynamic measurements, as well as computational simulations, are being employed to help the designers in converging to an optimal solution. However, some aerodynamic dynamic data are often impossible to obtain either computationally or experimentally through direct measurement. Novel experimental techniques have to be implemented in order to expand the analysis capability or to validate the design of specific configurations. A test technique that allows three degrees of freedom for investigating experimentally the dynamic behavior of parachute-payload systems is presented in this article. The system is utilized to investigate the effect of the parachute geometrical variables on the dynamic stability of the parachute-payload system. The cross-type parachute-payload systems that were tested exhibit three zones of different dynamic stability modes and the occurrence of dynamic instability for statically stable configurations. These results show the need for obtaining more dynamic data for the complete understanding of the dynamic behavior of closely coupled parachute-payload configurations.

Introduction

ROTATING parachute-payload systems have become common configurations for smart submunitions that are required to perform a complicated dynamic maneuver, such as searching for targets while descending. New goals were set for the aerodynamic design in order to obtain the desired performance characteristics that are mainly control of the rate of descent, the spin rate, and the instantaneous spatial position of the store. To help meet those goals, both computational and experimental tools were developed. Prediction of the dynamic behavior is used to shorten the design process and validate the performance of chosen configurations. In the past when only the trajectory of the c.g. of the system was required, a simulation based on the dynamics stability analysis of a single rigid mass was sufficient to provide adequate results.[1,2] The aerodynamic static coefficients required for such a simulation were obtained via conventional wind-tunnel tests, and verification could be achieved by direct measurements in drop tests. However, when the instantaneous position of the store, as well as its Eulerian angles are sought, the relative motion between the parachute and the payload has to be considered. This motion can be accounted for through an analysis based on two mechanically coupled masses. The nature of the coupling joint dictates the number of the degrees of freedom (DOF) necessary for the simulation. This number may vary from 9 DOF (6 DOF for the store and 3 for the parachute[3] in the case where the joint is assumed to behave as an ideal hinge), to 15 DOF when the joint is represented by a friction plate that has its own 6 DOF.[4] The multi-degrees-of-freedom simulations require inputs of the mechanical and aerodynamical static and dynamic properties of the configuration. The aerodynamic data should either be calculated or measured in controlled tests. Computations are unfortunately lagging in their ability to provide most of the aerodynamic data. Measurements in wind tunnels, in tow tanks, and drop tests are therefore the main source of static and limited dynamic data.[5–8] Innovative test techniques[9] have been used to obtain dynamic data that contributed to the simulation ability and to the verification of the predictions. Further modification of these techniques,[10,11] enabled the acquisition of the dynamic coefficients regarding the spin rate of rotating parachute-payload configurations. With the availability of the dynamic coefficients, the prediction of the dynamic behavior of some parachute-payload configurations in the steady-state descent conditions could be obtained. These predictions are based on a linear dependence between the aerodynamic coefficients and the spatial position of the system and its elements. The simulation can handle both stable and unstable configurations, and, as presented recently,[3] can incorporate the stochastic nature of the parachute-payload aerodynamics, by forcing stochastic disturbances into the wind velocity.

However, advanced parachute-payload systems, which require the parachute to perform as a flight control mechanism, exhibit dynamic patterns that cannot be fully apprehended by the approach of two coupled masses, and the dynamic data and analysis described in the previous chapter. The nature of the connection between the parachute and the payload is such that moments are transferred about the three axes and that the parachute cannot be regarded as a rigid body (elasticity of the suspension lines and that of the canopy play an important role in the dynamic behavior of the system). In such systems, more dynamic data is required in order to successfully predict the dynamic behavior. Such behavior patterns were monitored with a 3 degrees-of-freedom rig, and the effect of the geometrical variables on the dynamic stability of the systems was investigated.

Test Apparatus

A test system was designed to allow three rotational motions around the c.g. of the payload parachute system. The connection of the payload, shown schematically in Fig. 1, was built after a design by Nicolaides[13] for dynamic testing of a slender-missile configuration, and is a modified version of the apparatus used by Doherr[12] with 5 DOF. The payload can rotate continuously on low friction bearings located between the centerbody (black in Fig. 2) and the aft and front parts.

Received Feb. 21, 1993; presented as Paper 93-1205 at the RAeS/AIAA 12th Aerodynamic Decelerator Systems Technology Conference, London, England, UK, May 10–13, 1993; revision received Jan. 18, 1994; accepted for publication May 3, 1994.

*Senior Research Associate, Faculty of Aerospace Engineering. Member AIAA.

†Research Engineer, Faculty of Aerospace Engineering, Aerodynamic Research Center. Member AIAA.

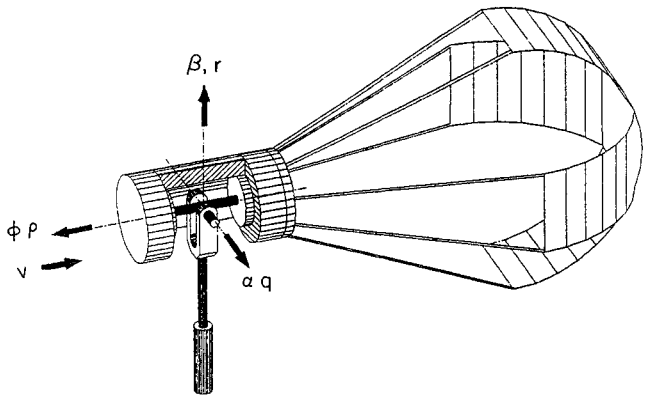

Fig. 1 Schematic drawing of the test rig.

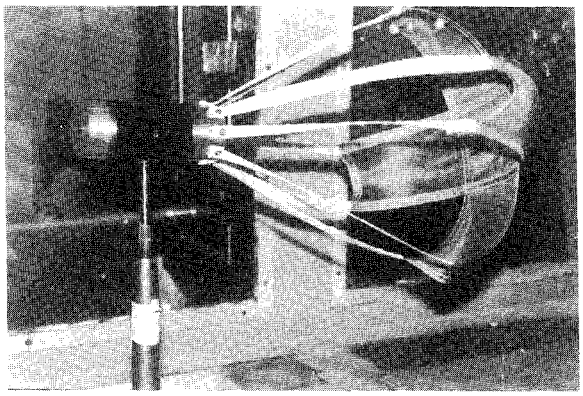

Fig. 2 Photograph of the test rig.

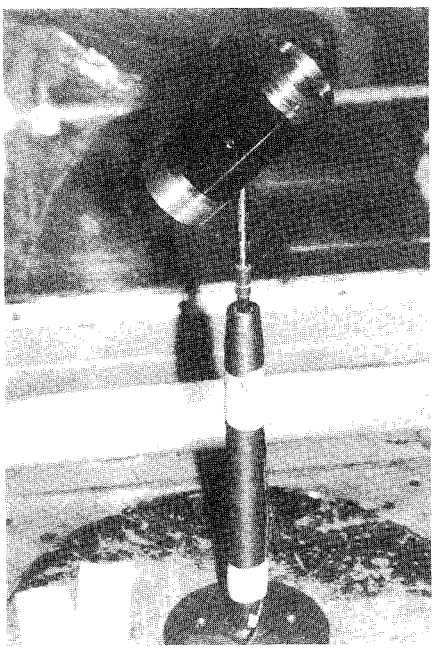

Fig. 3 Inflated model in the wind tunnel.

The roll rate p is measured by an optical sensor located inside the centerbody, the signal is transmitted via a thin fiberoptic line. Pitch motion in the α plane is limited to ± 60 deg with bearings located on the connecting fork (Fig. 1) between the strut and the payload model. The amplitude of the pitch angle is measured by a helical resistor. The strut is mounted on cylindrical bearings to provide the yawing motion in the β plane. A rotary variable displacement transducer (RVDT) measures the yaw angle.

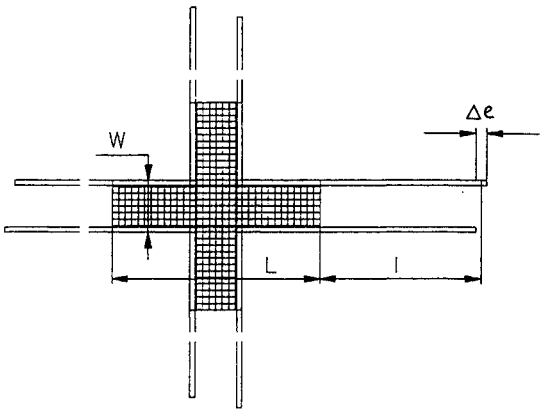

L/W - ASPECT RATIO

W/L - ARM RATIO

l/L - SUSPENSION LINE RATIO

Δe/L - STAGGERING RATIO

Fig. 4 Schematic drawing of cross-type parachute geometry.

The model tested is shown in Fig. 3. It consists of the payload, the centerbody of which is part of the test apparatus, a front interchangeable balancing section, and an aft section to which the cords of a cross-type parachute model are connected. Different cross-type parachutes were tested. They vary in their arm ratio (L/W) Fig. 4, and their suspension line ratio (l/L). Spin is generated by staggering the length of the parachute cords. Two different staggering ratios ($\Delta l/L$) were investigated. The various parachute configurations tested are presented in Table 1.

The connection between the store and parachute, as shown in Fig. 3, is capable of transferring the torque, so that both the payload and the parachute rotate at the same rate. The connection between the store and the cords behaves as a compound hinge, so that pitch and yaw moments can be partially transferred depending on the elasticity of the cords and of the canopy.

Test Results

The initial intention of the test rig was to investigate the aerodynamic interference between a geometrically nonsymmetrical payload and a rotating cross-type parachute. However, during the calibration runs of symmetrical configurations, large oscillations (± 15 deg) in both pitch and yaw were observed for configurations (load and parachute) that were statically stable. These results lead to a different avenue in the investigation, i.e., to define and understand the reasons for the different patterns of the dynamic behavior. The measurements included the pitch and yaw angles and the spin rate variation with time for a variety of configurations. The geometric variables are discussed in the test apparatus section. Typical output data are presented in Figs. 5–7. These figures represent the different types of dynamic behavior that have been observed in the tests. Each figure consists of three parts. The first a) shows the time history of the angle of the attack (pitch), the second b) shows the respective Fourier transform of the above time history, the third c) describes the combined longitudinal angular motion in the α, β plane. Figure 5 displays the data for a configuration that is stable at zero angle of attack. Small disturbances occur randomly; the magnitude of the fluctuations is small (± 2 deg); there is a dominant frequency of 4.6 Hz, but its magnitude is only slightly higher than the noise level. There exists no correlation between the pitch and yaw oscillations. Figure 6 presents the data for a dynamically unstable configuration. Fluctuations with large amplitudes (10–15 deg) are observed. They seem to occur in bursts and subside again. The dominant frequency remains

Table 1 Parachute configurations and parameters

Aspect ratio, W/L	l/L	$\Delta l/L$	Range α	Range β	rpm	Mode	Configuration
0.4	0.7	0.1	±10	±8	740	1–2	1346
	0.8	0.1	±4	±4	760	1	1345
	0.9	0.1	±15	±15	680	2	1347
	0.7	0.05	±15	±15	520	3	1375
	0.8	0.05	±20	±20	370	3	1369
	0.9	0.05	——	——	500	3	1374
	1.0	0.05	±20	±20	483	3	1370
0.33	0.7	0.1	±4	±4	730	1	1349
	0.8	0.1	±4	±4	710	1	1348
	0.9	0.1	±6	±6	720	1	1350
	1.0	0.1	±10	±10	648	2	1352
	0.7	0.05	±25	±25	530	3	1361
	0.8	0.05	±25	±25	520	3	1362
	0.9	0.05	±15	±15	520	2–3	1363
	1.0	0.05	±12	±12	485	2	1360
	1.1	0.05	±10	±10	585	2	1372
0.264	0.7	0.1	±2	±2	620	1	1357
	0.8	0.1	±2	±2	615	1	1359
	0.9	0.1	±4	±4	640	1	1358
	0.6	0.05	——	——	504	3	1368
	0.7	0.05	——	——	600	2	1366
	0.8	0.05	——	——	660	1	1365
	0.9	0.05	——	——	596	1	1364
	1.0	0.05	——	——	575	1	1367

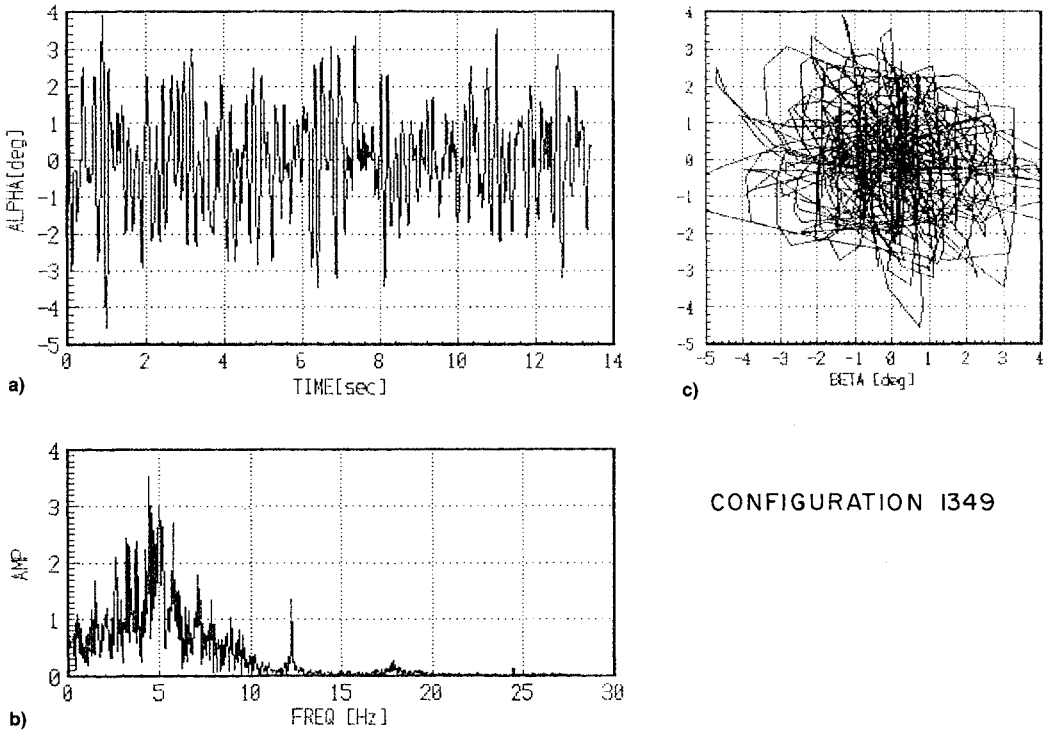

Fig. 5 Results for stable configuration: a) angle-of-attack variation with time, b) FFT of angle-of-attack variation with time, and c) angle of attack vs sideslip angle.

at 4.6 Hz, at a much larger amplitude than in the stable case, an effect of the spin frequency at 8.5 Hz becomes noticeable. The beginning of a conical motion can be tracked, but it is not fully established.

Figure 7 presents a fully developed steady conical motion, wherein the pitch and yaw angles behave in a coherent manner to create a circle when plotted against each other. The motion has a 15–20-deg half-cone angle! The dominant frequency is the spin frequency at 8.5 Hz with a magnitude almost triple that of the nonstable motion in Fig. 6. The various configurations tested exhibit one of the above dynamic patterns. The results are summarized in Table 2, and are graphically presented in Fig. 8. The different dynamic behavior patterns are typified as mode 1 (stable at zero), mode 2 (unstable), and mode 3 (stable coning motion). The trends of the effects of the three variables (spin rate, line suspension ratio, and arm ratio) on the dynamic stability mode are traced graphically.

In general, the three geometrical variables tested affect the dynamic stability, however, not always, in a similar manner to their effect on the static stability, as shown in previous

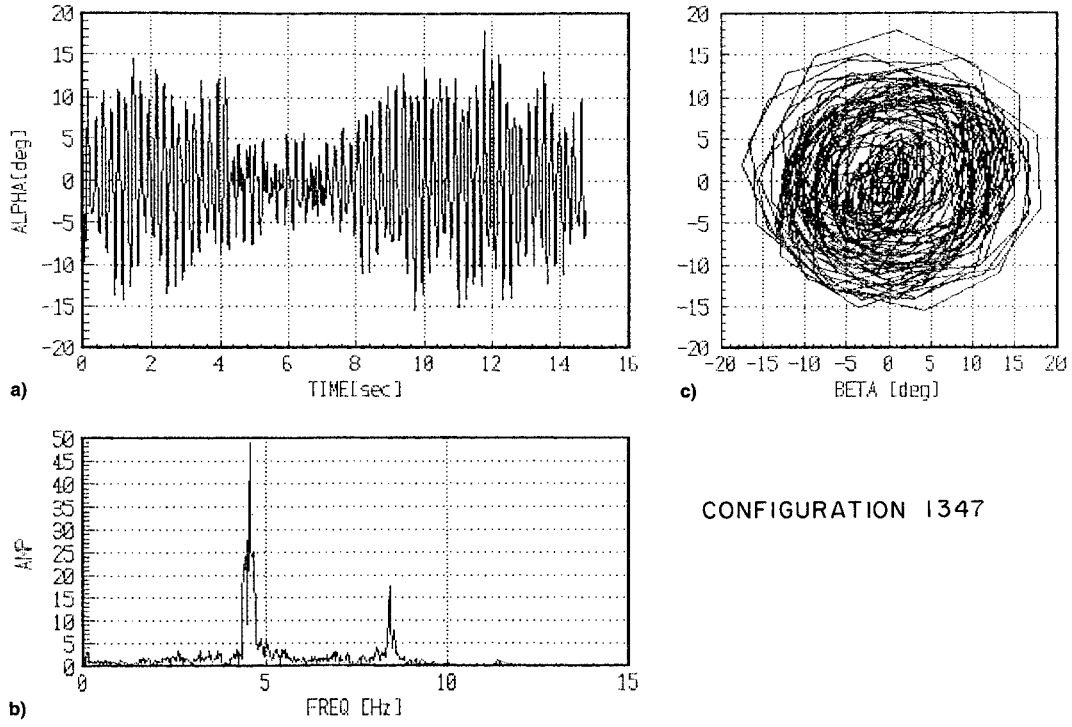

Fig. 6 Results for unstable configuration: a) angle-of-attack variation with time, b) FFT of angle-of-attack variation with time, and c) angle of attack vs sideslip angle.

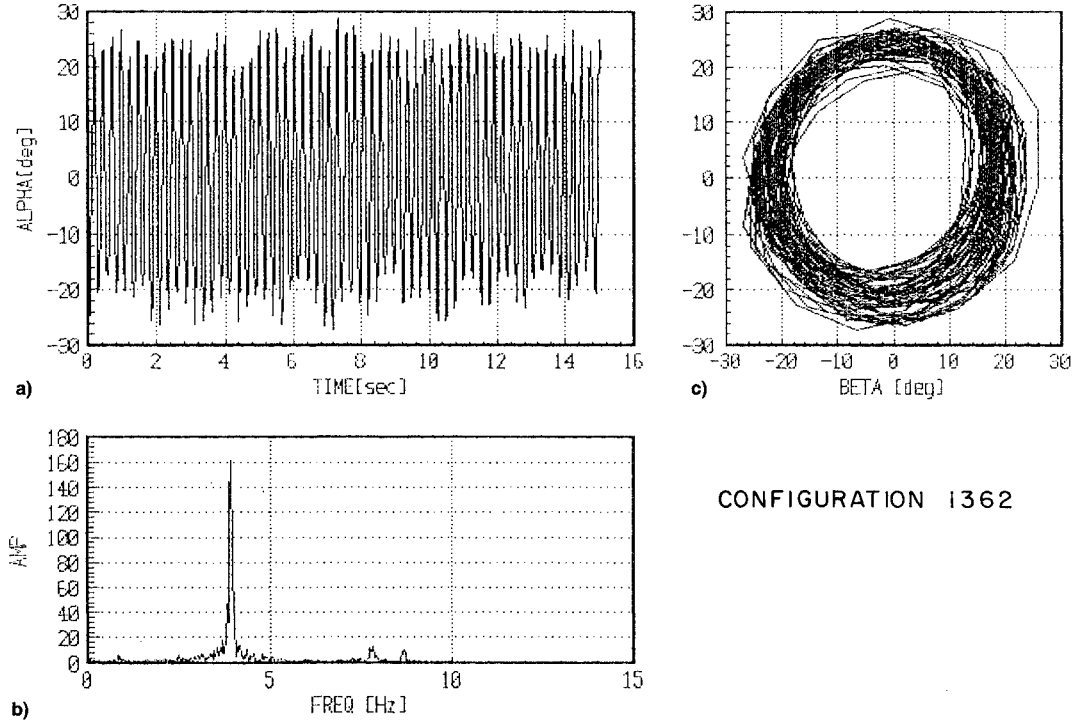

Fig. 7 Results for configuration at coning motion: a) angle-of-attack variation with time, b) FFT of angle-of-attack variation with time, and c) angle of attack vs sideslip angle.

investigations. In the range tested, the higher the canopy's aspect ratio, the higher the stability. Since the aspect-ratio represents the geometrical porosity, this is to be expected, similarly to the static test results of Shen and Cockrell.[14] However, the effect of the suspension line ratio (l/L) changes from increased stability with increased length for configurations at the lower spin rate, to decreasing stability (larger amplitude oscillations) with increased length at the higher spin rate as presented in Fig. 9. The spin rate effect is presented in Fig. 8. It changes the dynamic behavior from the coning mode 3 and the large oscillation mode 2, in the low spin rate, to stable mode 1 at high spin rate. The parachute with aspect ratio 0.4 performs a coning motion at the lower spin rate and large oscillations at the higher spin rate; at both rates (6 and 13 rps) the configuration is not stable. The other two canopies are stable (mode 1) at the high spin rate (12–13 rps), while moving from conical motion (mode 3) to large disordered motion (mode 2) at the lower spin rate (9–10 rps) depending on the other geometrical parameters, as discussed above.

Table 2 Dominant stability modes of the different dynamic motions

		$\Delta l/L = 0.05$					$\Delta l/L = 0.1$		
W/L		$l/L = 0.6$	$l/L = 0.7$	$l/L = 0.8$	$l/L = 0.9$	$l/L = 0.10$	$l/L = 0.7$	$l/L = 0.8$	$l/L = 0.9$
0.4	$f1$	—	4 (140)	4.5 (5)	—	—	5.3 (35)	5.5 (11)	4.5 (50)
	$f2$	—	8 (15)	7.8 (120)	—	8 (130)	9.5 (15)	9 (2.5)	8 (11.5)
	$f3$	—	8.5 (15)	6.2 (15)	—	—	13.3 (2)	12.8 (1)	—
0.33	$f1$	—	4 (140)	4 (160)	4 (68)	3.5 (22)	4.5 (5.5)	4.5 (8)	—
	$f2$	—	8 (15)	8 (15)	7.5 (28)	7 (6)	—	8 (2)	—
	$f3$	—	8.5 (15)	8.5 (15)	8.5 (8)	9.9 (1)	12.0 (0.8)	12 (1)	—
0.264	$f1$	—	3.5 (30)	4 (2.5)	5 (4)	4 (1.6)	—	—	—
	$f2$	—	5 (5)	8 (0.7)	7.8 (2)	—	—	—	—
	$f3$	8.5 (60)	10 (3)	11.5 (0.5)	10 (4)	9.5 (1.6)	—	—	—

Frequency in the Hz; in parentheses: relative magnitude of the FFT function.

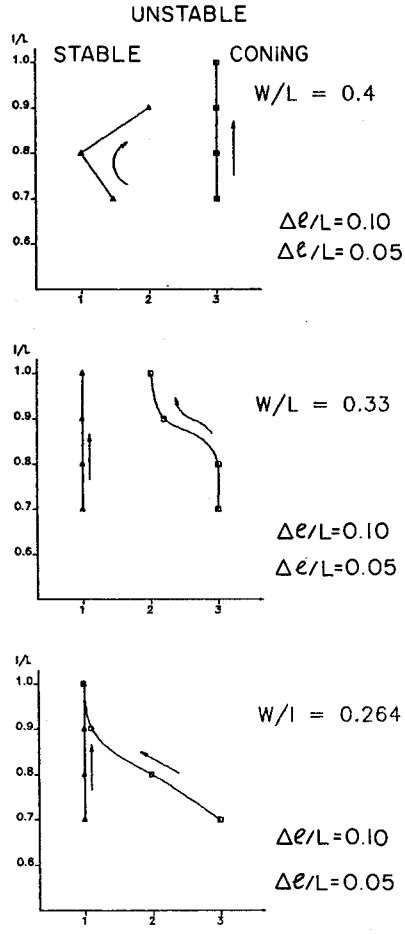

Fig. 8 Effect of the parachute geometrical variables on the dynamic stability.

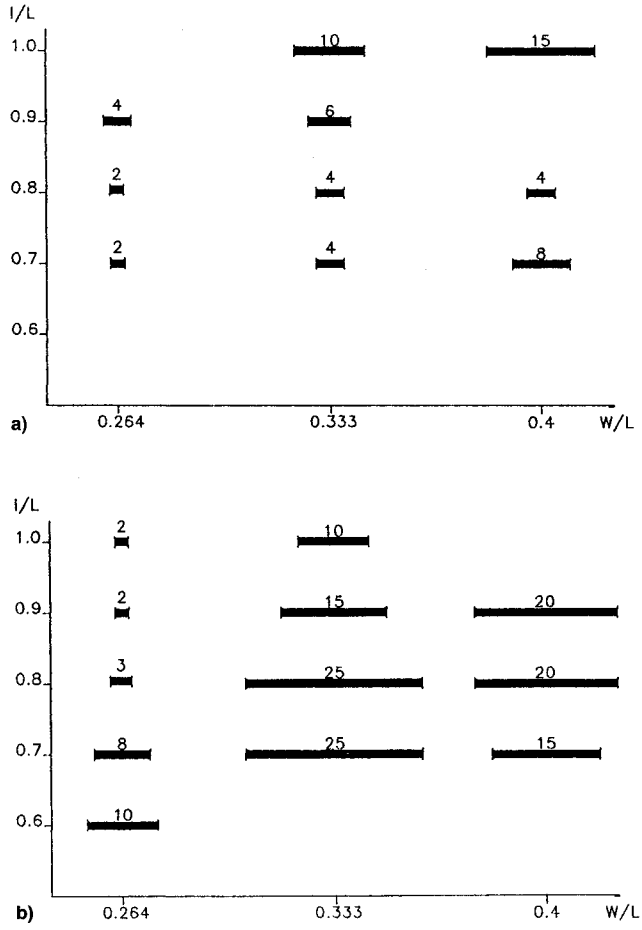

Fig. 9 Effect of suspension line ratio and arm ratio on magnitude of oscillations. Amplitude at a) high and b) low spin rates.

The data was processed in the frequency domain. Three frequencies appear to be more dominant. A frequency of 4–5 Hz ($f1$), a second frequency of 7–9 Hz ($f2$) and a third one 8–13 Hz ($f3$). The first two frequencies are related to the inertial and aerodynamic properties of the payload and the parachute. They vary slightly with the configuration changes, as the cords and canopy geometry affect the system's properties. The third frequency $f3$ is the spin rate frequency and depends strongly on the geometrical variables, mainly the spin generation by the stagger ratio, and the spin restoring moment C_{r_δ}, which is a function of the canopy aspect ratio and the suspension line ratio.

Typical results for the frequency power spectra are presented in Fig. 10. The dominant frequency for each configuration, and its amplitude, are summarized in Table 2.

In general, for stable configurations, $f1$ is the most noticeable frequency, however, its magnitude compared to the stochastic frequencies is small (4–8). The frequencies $f2$ and $f3$ are hardly noticed at all. In the cases of large oscillations (zone 2), $f1$ remains the dominant frequency, its amplitude compared to the noise, grows by an order of magnitude to (30–60). The frequencies $f2$ and $f3$ become apparent, although not as powerful as $f1$. It is interesting to note that the changes in the magnitude of $f2$ and $f3$ depend on the canopies aspect ratio. $f2$ and $f3$ are similarly intense for configurations with the smallest aspect ratio, while for these with the largest aspect ratio, $f2$ is more intense.

The frequency domain of the coning motions varies dramatically with the change of the aspect ratio. Configurations having the smallest aspect ratio (0.264) have the spin rate frequency $f(3)$ dominant, with $f(1)$ and $f(3)$ effects practically vanishing. The configurations with the medium aspect ratio (0.33) have $f(1)$ dominant with very high magnitude (>140), $f2$ and $f3$ are visible at a considerable lower intensity (~15).

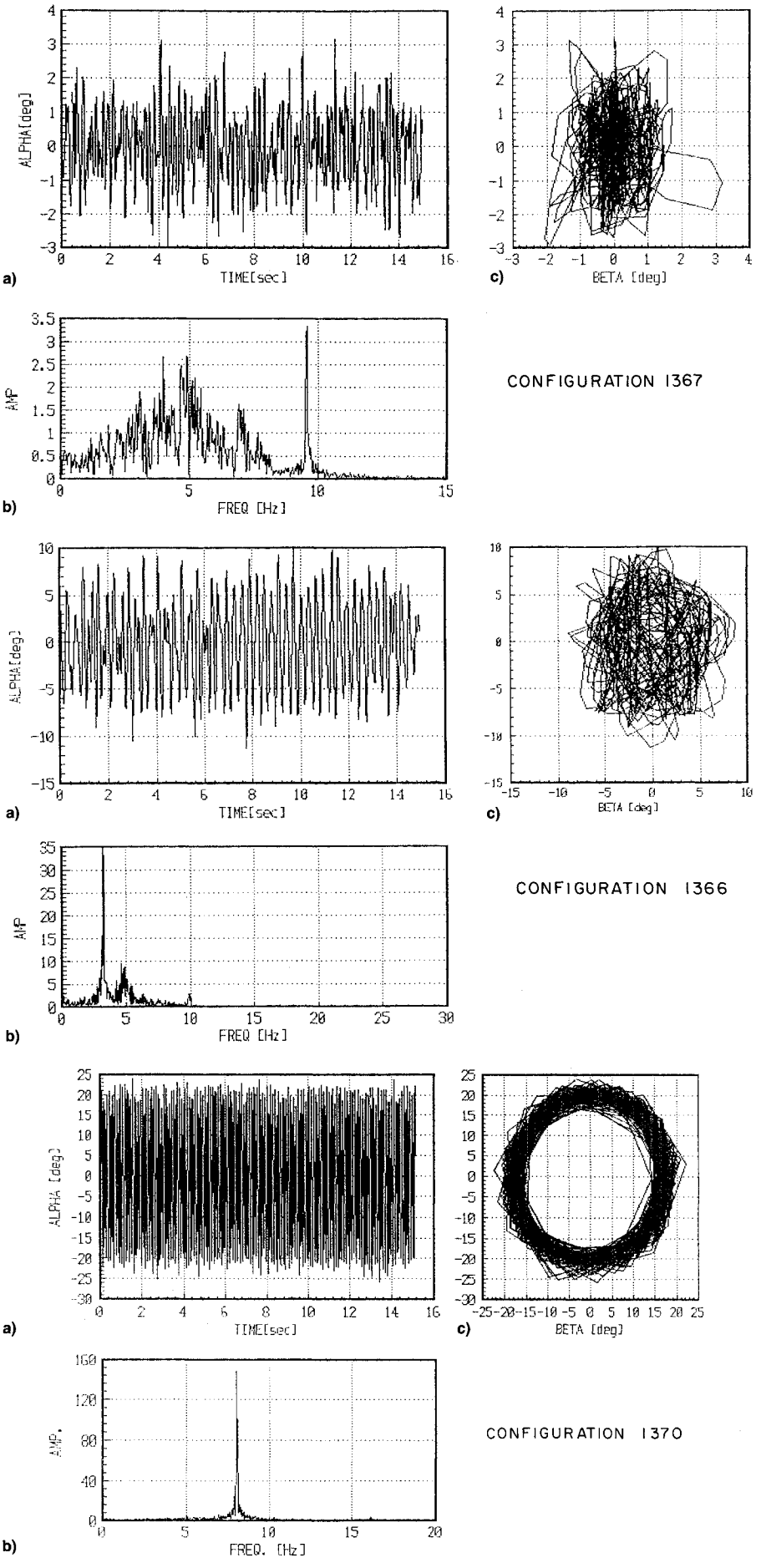

Fig. 10 Various stability modes: a) stable, b) unstable, and c) coning motion.

The larger aspect ratio configurations (0.4) undergoes the coning motion with $f2$ being the dominant frequency (>120), and $f1$ and $f3$ noticeable at a much lower level.

Discussion

The linearized analysis of a coupled parachute-payload system in the wind tunnel with 2 DOF of the pitching motion of the load and the parachute (presented by Doherr[17]), shows that two eigenvalues exist with complex eigenfrequencies. In the first eigenmode both parachute and payload oscillate into the same direction, and in the other eigenmode they oscillate in opposite directions. The dominant parameter of the complex eigenfrequency is the static stability of the parachute that depends on the parachute geometry (aspect ratio, arm ratio—Cockrell and Shen[14]). The lower eigenmode has small damping over the full range of the static stability. The damping of the higher eigenmode is zero at zero static stability and increases with increased static stability, i.e., at low static stability both modes can be easily excited by external disturbances. Parachutes with low static stability will perform chaotic pitch/yaw oscillations at zero angle of attack. Rotating parachutes are susceptible to roll-yaw coupling when the spin frequency gets in resonance with one of the oscillating eigenfrequencies.

Following this analysis the behavior of the three cross-type parachutes falls into a consistent pattern as follows:

Case 1: $W/L = 0.264$ or $L/W = 3.8$ (high static stability).

1) $\Delta l/L = 0.05$ (low roll rate): for long suspension lines oscillations with small amplitudes (mode 1) and with decreasing line length first large amplitudes (mode 2), then coning (mode 3). During the decrease of the line length the eigenfrequencies change until roll-yaw coupling occurs.

2) $\Delta l/L = 0.10$ (high spin rate): for all line lengths oscillations with only small amplitudes (mode 1). No roll-yaw coupling.

Case 2: $W/L = 0.33$ or $L/W = 3$ (reduced static stability).

1) $\Delta l/L = 0.05$ (low roll rate): for long lines oscillations with large amplitudes (mode 2), for shorter lines coning with large amplitudes due to roll-yaw coupling and reduced static stability (mode 3).

2) $\Delta l/L = 0.10$ (higher spin rate): for all line lengths oscillations with only small amplitudes (mode 1). No roll-yaw coupling.

Case 3: $W/L = -4$ or $L/W = 2.5$ (low static stability).

1) $\Delta l/L = 0.5$ (low roll rate): for all line lengths coning with large amplitudes due to roll-yaw coupling and low static stability (mode 3).

2) $\Delta l/L = 0.10$ (higher spin rate): oscillations with small to medium amplitudes (modes 1–2) due to low static stability accompanied by medium normal force fluctuations.

Concluding Remarks

The dynamic motion of a parachute-payload system in the wind tunnel, where the translatory motions do not exist, and the system is being constrained at the system c.g., is different from the motion experienced during actual flight. However, the main static and dynamic aerodynamical, as well as inertial properties manifest the same qualitative, if not quantitative, characteristics. The results of the wind-tunnel tests could be implemented for the design and analysis of the actual configurations.

A dynamic test rig that allows the angular motions of parachute-payload systems was used to investigate the dynamic stability of close-coupled parachute-payload configuration. The results indicate that such parachute-payload systems may develop in certain configurations large oscillations, and even a coning motion, although these configurations are statically stable. The linearized dynamic analysis, as presented by Doherr,[17] predicts the development of the large amplitudes and the coning motion, however, dynamic testing is often required to obtain the specific dynamic eigenmodes that influence specific designs, especially when the aerodynamic control of the trajectory through geometrical changes of the parachute is considered.

References

[1]Neustadt, M., et al., "A Parachute Recovery System Dynamic Analysis," *Journal of Spacecraft and Rockets*, Vol. 4, No. 3, 1967, pp. 321–326.

[2]White, F. M., and Wolf, D. F., "A Theory of Three-Dimensional Parachute Dynamic Stability," *Journal of Aircraft*, Vol. 5, No. 1, 1968, pp. 86–92.

[3]Doherr, K.-F., and Schilling, H., "9 DOF-Simulation of Rotating Parachute Systems," AIAA Paper 91-0877, April 1991.

[4]Pilash, D. W., Shen, Y. C., and Valero, N., "Parachute/Submunition System Coupled Dynamics," AIAA Paper 84-0784, April 1984.

[5]Doherr, K.-F., and Cockrell, D. J., "Preliminary Consideration of Parameter Identification Analysis from Parachute Aerodynamic Test Data," AIAA Paper 81-1940, Oct. 1981.

[6]Cockrell, D. J., Doherr, K.-F., and Polpitiye, S. J., "Further Experimental Determination of Parachute Virtual Mass Coefficients," AIAA Paper 84-0707, April 1984.

[7]Jorgensen, D. S., "Experimental Determination of the Input Parameters to the Parachute Equation of Motion," AIAA Paper 84-0798, April 1984.

[8]Cockrell, D. J., Shen, C. Q., Harwood, R. J., and Bartee, A. C., "Aerodynamic Forces Acting on Parachutes in Unsteady Motion and the Consequential Dynamic Stability Characteristics," AIAA Paper 86-2470, Oct. 1986.

[9]Doherr, K.-F., and Synofzik, R., "Investigation of Rotating Parachutes for Submunitions," AIAA Paper 86-2438, Oct. 1986.

[10]Shpund, Z., and Levin, D. B., "Improved Measurement of the Dynamic Loads Acting on Rotating Parachutes," AIAA Paper 86-2473, Oct. 1986.

[11]Shpund, Z., and Levin, D. B., "Measurement of the Static and Dynamic Coefficients of a Cross-Type Parachute in Subsonic Flow," AIAA Paper 91-0871, April 1991.

[12]Doherr, K.-F., "Theoretical and Experimental Investigation of Parachute-Load-System Dynamic Stability," AIAA Paper 75-1397, Nov. 1975.

[13]Nicolaides, J. D., and Eickenberry, R. S., "Dynamic Wind Tunnel Testing Techniques," AIAA Paper 66-752, April 1966.

[14]Shen, C. Q., and Cockrell, D. J., "Aerodynamic Characteristics and Flow Round Cross Parachute in Steady Motion," AIAA Paper 86-2458, Oct. 1986.

[15]Yavus, T., "Performance Prediction for Fully-Developed Parachute Canopies," AIAA Paper 86-2475, Oct. 1986.

[16]Sarpkaya, T., "Methods of Analysis for Flow Around Parachute Canopies," AIAA Paper 91-0825, April 1991.

[17]Doherr, K.-F., "Theoretical and Experimental Investigation of the Dynamic Behavior of Parachute-Load-Systems During Wind Tunnel Tests," DFVLR-FB 81-29, Aug. 1981.